A Switchable Dual-Frequency LCC-S-S Compensated Three-Coil WPT System for Mobile Desktop Charging With Constant Current and Constant Voltage Outputs

Haibing Wen, Jiayuan Li, Kehan Zhang, *Member, IEEE*, Peng Wang, Jiadong Yang, Xiaolong Zhou, Lei Yang, *Senior Member, IEEE*, Xiangqian Tong, *Member, IEEE*, and Baowei Song

***Abstract*—Wireless power transfer (WPT) system with three-coil has potential application prospect in mobile desktop charging, since it can effectively increase the transmission distance. In practical applications, the typical constant current (CC) and constant voltage (CV) two-stage charging mode for batteries is widely utilized. However, the batteries' equivalent resistance remarkably varies during the charging process, to realize both CC and CV outputs with different load conditions is a confronting problem for WPT system. To address the issue, a hybrid *LCC-S-S* compensation topology with an ac switch is proposed in this article. The CC/CV output characteristics can be fulfilled through the alternation of two fixed system operation frequencies and the switching of an ac switch at the receiver side. Besides, the zero phase angle (ZPA) conditions are also been met at the same time. A 50 W output experimental prototype is implemented to validate relevant theoretical analysis. The experimental results show that the CC/CV output characteristics are well maintained while the load resistance undergoes widely variation. Moreover, the ZPA operation can be achieved when receiver coil is misaligned. During the whole charging procedure, the peak power transfer efficiency can reach 91.9%.**

***Index Terms*—Constant current (CC), constant voltage (CV), LCC-S-S compensation topology, wireless power transfer (WPT), zero phase angle (ZPA).**

Received 29 July 2024; revised 12 October 2024 and 20 December 2024; accepted 17 January 2025. Date of publication 21 January 2025; date of current version 26 February 2025. This work was supported in part by the National Natural Science Foundation of China under Grant 52301403 and Grant 52171338, in part by the Natural Science Basic Research Plan in Shaanxi Province of China under Grant 2023-JC-QN-0475, in part by the China Postdoctoral Science Foundation under Grant 2021M702638, in part by the Xi'an Science and Technology Plan Project under Grant 24GXFW0052, and in part by the Beilin Science and Technology Plan Project under Grant GX2443. Recommended for publication by Associate Editor M. Ponce-Silva. *(Corresponding author: Haibing Wen.)*

Haibing Wen, Peng Wang, Jiadong Yang, Xiaolong Zhou, Lei Yang, and Xiangqian Tong are with the School of Electrical Engineering, Xi'an University of Technology, Xi'an 710048, China (e-mail: wenhaibing@xaut.edu.cn; 2221920013@stu.xaut.edu.cn; 2221920045@stu.xaut.edu.cn; 2231920044@stu.xaut.edu.cn; yanglei0930@xaut.edu.cn; xqtong@xaut.edu.cn).

Jiayuan Li, Kehan Zhang, and Baowei Song are with the School of Marine Science and Technology, Northwestern Polytechnical University, Xi'an 710072, China (e-mail: 3221712205@stu.xaut.edu.cn; 3210911022@stu.xaut.edu.cn; songbaowei@nwpu.edu.cn).

Color versions of one or more figures in this article are available at https://doi.org/10.1109/TPEL.2025.3532316.

Digital Object Identifier 10.1109/TPEL.2025.3532316

I. Introduction

As A contactless power supply approach, wireless power transfer (WPT) technology eliminates the complicated wire connections, thus the security and freedom of power transmission procedure are effectively enhanced. At present, it has been broadly utilized in numerous applications, such as electric vehicles, drones, underwater robots, automated guided vehicles, implantable electronic medical devices [1], [2], [3], [4], [5], etc. The application of WPT technology in mobile desktop charging could supply power to office equipment, such as tablet computer, projector and smartphone, while working, as shown in Fig. 1. It can enhance the office efficiency and user experience. Furthermore, the expenditure on built-in battery for mobile desktop consumer electronics can be reduced. In addition, the WPT system in mobile desktop charging is prone to install and hide under the table, complicated charging wires are eliminated, thus the cleanliness and aesthetic of workspace are significantly improved. Last but not least, the mismatching among desktop electronics equipment, power adapters and sockets of different manufacturers is expected to be effectively solved by the utilization of universal wireless charging system.

At present, Qi standard [6] is widely adopted in wireless charging system for portable consumer electronic equipment. However, the power transmission distance (the distance between transmitter coils and receiver coils) is a restriction that limit the application of WPT technology for mobile desktop electronics equipment. For the time being, the maximum coil-to-coil distance is up to 20 mm for existing Qi certified wireless charging devices. Whereas, the thickness of tabletop is as much as 50 mm, especially for some high-grade office furniture. In order to install transmitter coil, making a cavity in the tabletop is inevitable. Unfortunately, the destructive assembly process is unallowed for office furniture manufactures. WPT system with intermediate coil is an effective approach to enlarge the power transmission distance while mitigate the reduction of power transfer efficiency [7], [8]. In order to supply power to consumer electronics in mobile desktop charging scenarios, a WPT system with three-coil configuration is introduced in this article.

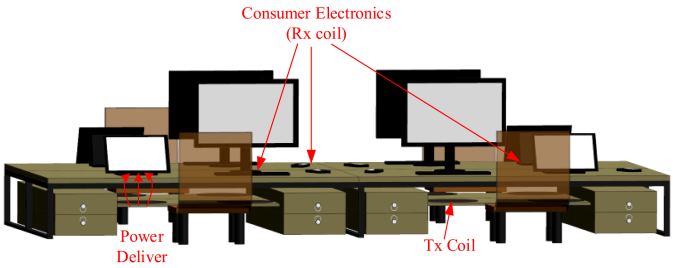

Fig. 1. WPT system for mobile desktop consumer electronics.

Currently, lithium-ion batteries, which have the advantages of high-performance and low-cost, are selected as power source for most consumer electronics. To improve the durability, safety and efficiency of batteries, the typical two-stage charging process are widely employed [9]. That is, in the initial charging procedure, the constant current (CC) phase is adopted, then the constant voltage (CV) charging stage begins as the upper voltage limit reaches, and the charging process ends when the current drops to the lower limit. The batteries' equivalent resistance varies noticeably during the whole charging process, that means it is essential to provide CC and CV output characteristics for the WPT system independent of load resistance. Besides, as the key to keep the efficient operation of system, zero phase angle (ZPA) characteristic should be preserved during the whole charging process.

Up to now, the reported approaches to achieve CC and CV charging modes for WPT system are mainly separated into three kinds. The most commonly used CC and CV realization means under unvarying compensation topology were proposed in [10], [11], and [12], including phase shifting control, dc–dc converter and frequency tuning control. By means of adapting the phase shifting angle of power converter, to be specific, regulate the phase shifting angle of four MOSFETs in the inverter or diodes in the rectifier through real-time data of the load voltage and current, the controllable CC and CV outputs could be achieved [10]. However, the power loss caused by hard ON-OFF switch is inevitable. Frequency tuning control may bring frequency splitting phenomenon to the system, thus decrease the output stability [11]. The dc–dc converter was introduced to adjust the output voltage and current of the *Tx* side or *Rx* side, but the extra power loss and volume growth brought by passive components of dc–dc converter are nonnegligible [12]. In addition, the abovementioned methods are closely dependent on the real-time communication between the primary side and secondary side. The interruption or postponement of communication will significantly influence the output characteristic of WPT system.

Second, by virtue of the alternation between different compensation topologies, CC and CV output characteristic can be acquired in three-coil WPT system [13]. One or more switches are employed to change the CC/CV charging mode, since one compensation topology has CC output characteristic, and the other compensation topology exhibits CV output characteristic under the same operation frequency. A two/three-coil hybrid configuration WPT system was proposed to realize CC and CV charging mode by Chen et al. [14]. The CC charging mode is obtained with two-coil topology, conversely, the CV output is achieved when the system operates in three-coil topology. The alternation between different operating modes requires two ac switches. Li et al. [7] put forward a combination WPT configuration of *S-S-S* topology with CV characteristic and *S-S-LCC* topology with CC output, two ac switches are utilized to realize the converting from CC to CV charging mode. The ac switches must turn at the same time, otherwise it would bring reactive power loss to the system. In addition, the mentioned method introduces excessive passive components, increasing the volume, weight and cost. To avoid this situation, a novel reconfigurable topology with one ac switch was proposed in [15]. In the mentioned system, the transmitting coil can be reconfigured as one winding or two windings, thus the CC output is achieved with two-coil structure and the CV output is obtained with three-coil structure. However, in the proposed transmitting coil, the number of turns of one winding is much smaller than the other. This special winding method is actually proposed for traditional WPT system, and it is not applicable to three-coil WPT system. A dual switchable WPT system including intermediate coil was proposed in [16], the CC and CV output characteristics under a constant resonant frequency are achieved by the introduction of two switches. However, this method adopted an auxiliary inductor in the transmitter side, it increased system volume and loss. Xu et al. [17] proposed an auxiliary circuit to realize automatic seamless CC-to-CV transition in three-coil WPT system. But four additional diodes of the auxiliary circuit result in the increment of power loss and volume.

Third, in three-coil WPT system, CC and CV output characteristics can be realized under two operating frequencies with the same topology [18]. Yang et al. [19] proposed a CC and CV outputs WPT system with *S-S-S* topology, the system works at two different frequencies, ZPA operation is also obtained. Nevertheless, the low power transfer efficiency in CV mode makes it difficult to apply in practice. To solve this problem, a novel *S-S-P* topology WPT system was put forward with higher power transfer efficiency in CV charging mode [20]. However, the above two topologies could only achieve ZPA characteristic under constant coupling coefficient between three coils, it is essential to redesign the parameters of the compensation topology when the misalignments occur between the transmitter coil and receiver coil. The complexity of the system is increased while its reliability is reduced.

The WPT system with *S-CLCC* topology has the ability to output CC and CV characteristics, it is achieved by the switching of two fixed frequencies, moreover, the resonant frequencies are independent of mutual inductance [21]. Unfortunately, this topology is not applicable to WPT system with intermediate coil and the parameter design process is complex. Therefore, to fill this gap, a hybrid *LCC-S-S* topology is proposed in this article to address the abovementioned issue for three-coil WPT system. The CC/CV output characteristics can be achieved independent of load resistance under two fixed frequencies, and

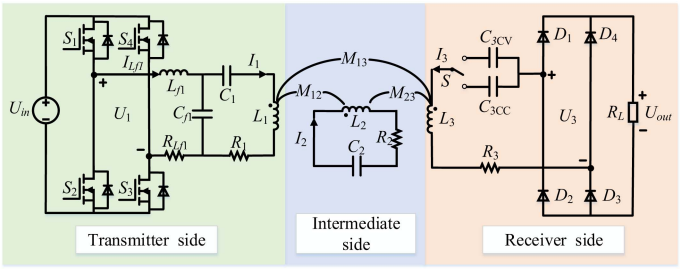

Fig. 2. Circuit diagram of the proposed three-coil WPT system.

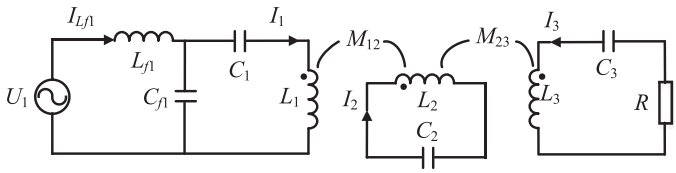

Fig. 3. Simplified circuit of WPT system with intermediate coil.

ZPA operation is not affected by the position variation of Rx coil in the proposed WPT system.

The rest of this article is organized as follows. The detail theoretical analysis of proposed three-coil WPT system with LCC-S-S compensation topology to obtain CC/CV output characteristics, and the parameter design process are presented in Section II. The magnetic coupling structure and simulation verification are given in Section III, the results demonstrate that the CC/CV output characteristics is acquired when the load resistance undergoes widely variation, moreover, the ZPA operation is maintained under different coupling coefficients. In this section, the experimental prototype is demonstrated, and the output characteristic of proposed WPT system with intermediate coil is verified by relevant experiments. Finally, Section V concludes this article.

II. Theoretical Analysis

A. Equivalent Circuit Model

The circuit diagram of the proposed WPT system is shown in Fig. 2. The dc source U_{in}, the inverter, the resonant network, the magnetic coupler, the passive rectifier and the battery load are mainly included. The inverter is made up of four power MOSFETs (S_1-S_4). The inductance of *Tx* coil, intermediate coil and *Rx* coil, named as L_1, L_2, and L_3, respectively. M_{12} represents the mutual inductance between *Tx* coil and intermediate coil, M_{13} stands for the mutual inductance between *Tx* coil and *Rx* coil, while M_{23} is the mutual inductance between intermediate coil and Rx coil. L_{f1}, C_{f1}, and C_1 are the compensation inductance and capacitors in the transmitter side, C_2 represents the compensation capacitor in series with intermediate coil. The compensation capacitors C_{3CV} and C_{3CC} are connected in series with *Rx* coil, *S* is the ac switch to control capacitor alternation. Moreover, a passive rectifier with four Schottky diodes (D_1-D_4) is employed in the receiver sssimilar side.

To facilitate the analysis of basic characteristics of the circuit, all of the high-order harmonics and the parasitic resistance of all passive components are ignored. Besides, mutual inductance M_{13} is negligible and omitted in the following theoretical analysis, considering the distance between *Tx* coil and *Rx* coil [22]. Fig. 3 demonstrates the simplified circuit of WPT system with intermediate coil.

In the above-mentioned simplified circuit model, *R* is the equivalent resistance considering the whole rectifier and load stage. It can be defined as [22]

$$R = \frac{8}{\pi^2} R_L. \tag{1}$$

Based on the Kirchhoff's voltage law, the following equations can be obtained:

$$\begin{cases} \dot{U}_1 = X_{Lf1}\dot{I}_{Lf1} + X_{Cf1}\dot{I}_1 \\ 0 = X_{Cf1}\dot{I}_{Lf1} + X_1\dot{I}_1 + X_{M12}\dot{I}_2 \\ 0 = X_{M12}\dot{I}_1 + X_2\dot{I}_2 + X_{M23}\dot{I}_3 \\ 0 = X_{M23}\dot{I}_2 + (X_3 + R)\dot{I}_3 \end{cases} \tag{2}$$

where $\dot{I}_{Lf1}$, $\dot{I}_1$, $\dot{I}_2$, and $\dot{I}_3$ denote the current flowing through each inductance, respectively. Besides, the reactance in (2) are defined as following:

$$\begin{cases} X_{Lf1} = j\omega L_{f1} + 1/(j\omega C_{f1}) \\ X_1 j\omega L_1 + 1/(j\omega C_1) + 1/(j\omega C_{f1}) \\ X_2 j\omega L_2 + 1/(j\omega C_2) \\ X_3 j\omega L_3 + 1/(j\omega C_3) \end{cases} \tag{3}$$

$$\begin{cases} X_{Cf1} = 1/(j\omega C_{f1}) \\ X_{M12} = j\omega M_{12} \\ X_{M23} = j\omega M_{23}. \end{cases} \tag{4}$$

In the above equations, ω stands for system operating angular frequency. By regulating the system operating frequency, the abovementioned reactance value can be changed. However, all reactance in (3) can be equal to 0 (when the operating frequency is consistent with the resonant frequency), on the contrary, all reactance in (4) cannot be 0 at any system operating frequencies. By solving (2), the input current I_{Lf1} and output current I_3 can be deduced as

$$\begin{cases} \dot{I}_{Lf1} = \frac{(X_1X_{M23}^2 - X_2X_3 + X_3X_{M12}^2) + (X_{M12}^2 - X_1X_2)R}{\mathrm{A} + \mathrm{B}R}\dot{U}_1 \\ \dot{I}_3 = \frac{X_{Cf1}X_{M12}X_{M23}}{\mathrm{A} + \mathrm{B}R}\dot{U}_1 \end{cases} \tag{5}$$

where A and B are expressed as

$$\begin{cases} \mathrm{A} = (X_1X_{Lf1} - X_{Cf1}^2)X_{M23}^2 + (X_{M12}^2 - X_1X_2)X_3X_{Lf1} \\ \qquad + X_2X_3X_{Cf1}^2 \\ \mathrm{B} = X_{Lf1}X_{M12}^2 + X_2X_{Cf1}^2 - X_1X_2X_{Lf1} \end{cases}. \tag{6}$$

Then, the transconductance G_{IU}, voltage gain G_{UU} and input impedance Z_{in} are calculated as follows:

$$G_{IU} = \left|\frac{I_3}{U_1}\right| = \left|\frac{X_{Cf1}X_{M12}X_{M23}}{\mathrm{A}+\mathrm{B}R}\right| \tag{7}$$

$$G_{UU} = \left|\frac{I_3 R}{U_1}\right| = \left|\frac{X_{Cf1}X_{M12}X_{M23}}{\mathrm{A}R^{-1}+\mathrm{B}}\right| \tag{8}$$

$$Z_{in} = \left|\frac{\mathrm{A}+\mathrm{B}R}{X_3X_{M12}^2 + X_1X_{M23}^2 - X_1X_2X_3 + (X_{M12}^2 - X_1X_2)R}\right|. \tag{9}$$

It can be seen from (6) and (7) that the transconductance gain of the system independent of load resistance can be obtained by making the coefficient B equal to 0. Similarly, the voltage gain independent of load resistance can be achieved when $A = 0$. However, to maintain the system's ZPA conditions and guarantee the above characteristics not be affected by the variation of mutual inductance, more detailed theoretical analysis will be discussed in the following. Besides, M_{12} is considered as fixed value in the following analysis, because it is not impacted by the misalignment of *Rx* coil.

B. Analysis of CC Charging Mode With ZPA Condition

Based on (6), when $B = 0$, the output current gain of WPT system is not change with load resistance, and thus it is indicated that the CC charging mode can be achieved. Therefore, the realization conditions of CC charging mode are as follows:

$$\mathrm{B} = X_{Lf1}X_{M12}^2 + X_2X_{Cf1}^2 - X_1X_2X_{Lf1} = 0. \tag{10}$$

Besides, combined (8), ZPA condition in CC charging mode can be achieved when $X_3X_{M12}^2 + X_1X_{M23}^2 - X_1X_2X_3 = 0$ is satisfied. To ensure the above realization conditions are not affected by M_{23}, $X_1 = 0$ and $X_3 = 0$ should be established. Then, (10) is rewritten as

$$\mathrm{B} = X_{Lf1}X_{M12}^2 + X_2X_{Cf1}^2 = 0 \tag{11}$$

$$X_2 = -\frac{X_{Lf1}X_{M12}^2}{X_{Cf1}^2}. \tag{12}$$

Combined with above analysis and (3) and (4), the following equation can be obtained to achieve CC mode with ZPA condition:

$$\begin{cases} j\omega_{\mathrm{CC}}L_2 + \frac{1}{j\omega_{\mathrm{CC}}C_2} = \frac{\left(j\omega_{\mathrm{CC}}L_{f1} + \frac{1}{j\omega_{\mathrm{CC}}C_{f1}}\right)(j\omega_{\mathrm{CC}}M_{12})^2}{\left(\frac{1}{j\omega_{\mathrm{CC}}C_{f1}}\right)^2} \\ j\omega_{\mathrm{CC}}L_1 + \frac{1}{j\omega_{\mathrm{CC}}C_1} + \frac{1}{j\omega_{\mathrm{CC}}C_{f1}} = 0 \\ j\omega_{\mathrm{CC}}L_3 + \frac{1}{j\omega_{\mathrm{CC}}C_3} = 0 \end{cases} \tag{13}$$

where ω_{CC} is the system operating angular frequency when the WPT system works in CC charging mode. There are two solutions for (12), $X_2 = X_{Lf1} = 0$ and X_2 and $X_{Lf1} \neq 0$. For solution ii, combining (13), when the values of four inductance and system operating frequency ω_{CC} in CC charging mode are fixed, the parameter of compensation capacitance is related to mutual inductance M_{12}, which would increase the complexity of system design and construction. However, for solution *i*, the values of all compensation capacitances are only associated with four inductance and system operating frequency ω_{CC}, and can be calculated as

$$\begin{cases} C_{f1} = \frac{1}{\omega_{\mathrm{CC}}^2 L_{f1}} \\ C_1 = \frac{1}{\omega_{\mathrm{CC}}^2 (L_1 - L_{f1})} \\ C_2 = \frac{1}{\omega_{\mathrm{CC}}^2 L_2} \\ C_3 = \frac{1}{\omega_{\mathrm{CC}}^2 L_3} \end{cases}. \tag{14}$$

Equations (7) and (9) can be rewritten as

$$G_{IU}(\omega_{\mathrm{CC}}) = \frac{\omega_{\mathrm{CC}}C_{f1}M_{12}}{M_{23}} \tag{15}$$

$$Z_{\mathrm{in}}(\omega_{\mathrm{CC}}) = \frac{M_{23}^2}{\omega^2 C_{f1}^2 M_{12}^2 R}. \tag{16}$$

Equations (15) and (16) are the output current gain and system input impedance in CC charging mode, respectively. From (15) and above analysis, the output current gain is independent of load resistance *R*. Similarly, from (16), ZPA condition in CC charging mode could maintain independent of M_{23}. Besides, the current flowing through each inductor in CC charging mode can be calculated as follows:

$$\begin{cases} \dot{I}_{Lf1}(\mathrm{CC}) = \frac{\omega_{\mathrm{CV}}^2 C_{f1}^2 M_{12}^2 M_{23}^2}{M_{23}^2}\dot{U}_1 R \\ \dot{I}_1(\mathrm{CC}) = j\omega_{\mathrm{CC}}C_{f1}\dot{U}_1 \\ \dot{I}_2(\mathrm{CC}) = -j\frac{\omega_{CC}C_{f1}M_{12}}{M_{23}^2}\dot{U}_1 R \\ \dot{I}_3(\mathrm{CC}) = -\frac{\omega_{\mathrm{CC}}C_{f1}M_{12}}{M_{23}}\dot{U}_1 \end{cases}. \tag{17}$$

Combined with (17), the power transfer efficiency η(CC) of the proposed WPT system in CC charging mode is expressed as

$$\eta(\mathrm{CC}) = \frac{|I_3(\mathrm{CC})|^2 R}{|I_{Lf1}(\mathrm{CC})|^2 R_{Lf1} + |I_1(\mathrm{CC})|^2 R_1 + |I_2(\mathrm{CC})|^2 R_2 + |I_3(\mathrm{CC})|^2 (R_3 + R)}. \tag{18}$$

C. Analysis of CV Charging Mode With ZPA Condition

Similar analysis can also be adopted in CV charging mode. Based on (8), when $A = 0$, the output voltage gain will not vary with the alteration of load resistance, it can be inferred that the CV output characteristic would be obtained. Besides, combined (9), ZPA condition can be achieved when $X_{M12}^2 - X_1X_2 = 0$. Substitute the above equation into (6), and simplification, A is rewritten as

$$\mathrm{A} = \left(X_1X_{Lf1} - X_{Cf1}^2\right)X_{M23}^2 + X_2X_3X_{Cf1}^2. \tag{19}$$

From (19), to ensure $\mathrm{A} = 0$ is not affected by the value of M_{23}, $X_1X_{Lf1} - X_{Cf1}^2 = 0$ and $X_3 = 0$ should be established. Combined with (3), the following (20) can be obtained to achieve

CV charging mode with ZPA condition

$$\begin{cases} (\omega_{\mathrm{CV}}M_{12})^2=\left(\omega_{\mathrm{CV}}L_1-\frac{1}{\omega_{\mathrm{CV}}C_1}-\frac{1}{\omega_{\mathrm{CV}}C_{f1}}\right)\left(\omega_{\mathrm{CV}}L_2-\frac{1}{\omega_{\mathrm{CV}}C_2}\right) \\ \left(\frac{1}{\omega_{\mathrm{CV}}C_{f1}}\right)^2=\left(\omega_{\mathrm{CV}}L_1-\frac{1}{\omega_{\mathrm{CV}}C_1}-\frac{1}{\omega_{\mathrm{CV}}C_{f1}}\right)\left(\omega_{\mathrm{CV}}L_{f1}-\frac{1}{\omega_{\mathrm{CV}}C_{f1}}\right) \\ \omega_{\mathrm{CV}}L_3-\frac{1}{\omega_{\mathrm{CV}}C_3}=0 \end{cases} \tag{20}$$

where ω_{CV} is the system operation angular frequency while the WPT system works in CV charging mode. Then, substitute (14) into (20) and simplification, the following equations can be obtained.

$$(\omega_{\mathrm{CV}}M_{12})^2=\left(\omega_{\mathrm{CV}}L_1-\frac{\omega_{\mathrm{cc}}^2(L_1-L_{f1})}{\omega_{\mathrm{CV}}}-\frac{\omega_{\mathrm{cc}}^2L_{f1}}{\omega_{\mathrm{CV}}}\right)\times\left(\omega_{\mathrm{CV}}L_2-\frac{\omega_{\mathrm{cc}}^2L_2}{\omega_{\mathrm{CV}}}\right) \tag{21}$$

$$\left(\frac{\omega_{\mathrm{cc}}^2L_{f1}}{\omega_{\mathrm{CV}}}\right)^2=\left(\omega_{\mathrm{CV}}L_1-\frac{\omega_{\mathrm{cc}}^2(L_1-L_{f1})}{\omega_{\mathrm{CV}}}-\frac{\omega_{\mathrm{cc}}^2L_{f1}}{\omega_{\mathrm{CV}}}\right)\times\left(\omega_{\mathrm{CV}}L_{f1}-\frac{\omega_{\mathrm{cc}}^2L_{f1}}{\omega_{\mathrm{CV}}}\right) \tag{22}$$

$$\omega_{\mathrm{CV}}L_3-\frac{\omega_{\mathrm{cc}}^2L_3}{\omega_{\mathrm{CV}}}=0. \tag{23}$$

Equations (21) and (22) have two solutions

$$\begin{cases} \text{Solution 1}: \omega_{\mathrm{CV1}}=\sqrt{\frac{1}{1+k_{12}}}\omega_{\mathrm{CC}}, L_{f1,1}=L_1\left(\frac{k_{12}}{k_{12}+1}\right)^2 \\ \text{Solution 2}: \omega_{\mathrm{CV2}}=\sqrt{\frac{1}{1-k_{12}}}\omega_{\mathrm{CC}}, L_{f1,2}=L_1\left(\frac{k_{12}}{k_{12}-1}\right)^2 \end{cases} \tag{24}$$

where k_{12} is the coupling coefficient between *Tx* coil and intermediate coil and express as $k_{12}=M_{12}/\sqrt{L_1L_2}$. In addition, (23) cannot be satisfied when $\omega_{\mathrm{CC}}\neq\omega_{\mathrm{CV}}$. Therefore, the value of C_3 in different charging modes can be calculated as following equations and changing-over through ac switch *S*, as shown in Fig. 2

$$\begin{cases} C_{3\mathrm{CC}}=\frac{1}{\omega_{\mathrm{cc}}^2L_3} \\ C_{3\mathrm{CV}}=\frac{1}{(\omega_{\mathrm{CV}}^2-\omega_{\mathrm{cc}}^2)L_3} \end{cases}. \tag{25}$$

Equations (8) and (9) can be rewritten as

$$G_{\mathrm{UU}}=\left|\frac{(\omega_{\mathrm{CC}}^2-\omega_{\mathrm{CV}}^2)M_{23}}{(\omega_{\mathrm{CC}}\omega_{\mathrm{CV}}C_{f1})^2M_{12}}\right| \tag{26}$$

$$Z_{\mathrm{in}}=\frac{L_2L_{f1}^2\omega_{\mathrm{CC}}^4}{L_1M_{23}^2\omega_{\mathrm{CV}}^4}R. \tag{27}$$

Equation (26) denotes the output voltage gain under CV charging mode, while (27) represents the input impedance. (26) and above analysis indicate that the variation of load resistance does not influence the output voltage gain under CV operation mode. Similarly, from (27), ZPA condition in CV operation could be maintained independent of M_{23}. Besides, the current flowing through each inductor in CV charging mode can be calculated as follows:

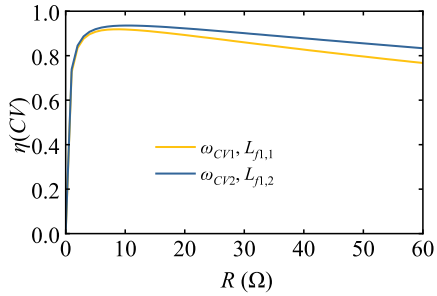

Fig. 4. Power transfer efficiency with two solutions.

$$\begin{cases} \dot{I}_{Lf1}(\mathrm{CV})=\frac{\omega_{\mathrm{CC}}^2C_{f1}^2M_{12}^2}{M_{23}^2}\dot{U}_1R \\ \dot{I}_1(\mathrm{CV})=\frac{\omega_{\mathrm{CV}}^2M_{23}^2}{\frac{L_2}{C_{f1}}-\frac{1}{\omega_{\mathrm{CV}}^2C_2C_{f1}}}\frac{\dot{U}_1}{R}-j\omega_{CV}C_{f1}\dot{U}_1 \\ \dot{I}_2(\mathrm{CV})=-j\frac{\omega_{\mathrm{CV}}M_{12}}{\frac{L_2}{C_{f1}}-\frac{1}{\omega_{\mathrm{CV}}^2C_2C_{f1}}}\dot{U}_1 \\ \dot{I}_3(\mathrm{CV})=-\frac{\omega_{\mathrm{CV}}^2M_{12}M_{23}}{\frac{L_2}{C_{f1}}-\frac{1}{\omega_{\mathrm{CV}}^2C_2C_{f1}}}\frac{\dot{U}_1}{R} \end{cases}. \tag{28}$$

Combined with (28), the proposed WPT system's power transfer efficiency η(CV) under CV charging mode could be denoted as

$$\eta(\mathrm{CV})=\frac{|I_3(\mathrm{CV})|^2R}{|I_{Lf1}(\mathrm{CV})|^2R_{Lf1}+|I_1(\mathrm{CV})|^2R_1+|I_2(\mathrm{CV})|^2R_2+|I_3(\mathrm{CV})|^2(R_3+R)}. \tag{29}$$

Under the condition of ignoring skin effects, the efficiency analysis of the whole system in CV charging pattern with two cases from (24) is displayed in Fig. 4. When system works in CV operation pattern, the power transfer efficiency in solution 2 is better than solution 1. Therefore, $\omega_{\mathrm{CV2}}=\sqrt{\frac{1}{1-k_{12}}}\omega_{\mathrm{CC}}, L_{f1,2}=L_1\left(\frac{k_{12}}{k_{12}-1}\right)^2$ is selected for CV charging mode.

D. Parameter Design Process and Switching Control Flowchart

Fig. 5 demonstrates the compensation parameter design process of the proposed WPT system. First, self-inductance L_1, L_2, L_3 and mutual inductance M_{12} should be determined according to the magnetic coupler structure and preset the operating frequency ω_{CC} in CC charging phase. Secondly, combing (14) and (25), calculate the values of compensation capacitance C_{f1}, C_1, C_2 and $C_{3\mathrm{CC}}$. Third, determine the compensation inductance L_{f1} and the operating frequency ω_{CV} in CV charging mode by (24). Lastly, according to (25), the value of compensation capacitance $C_{3\mathrm{CV}}$ is defined. The above process configures all compensation parameter values in the *LCC-S-S* topology and the system's operating frequencies in CC and CV charging mode.

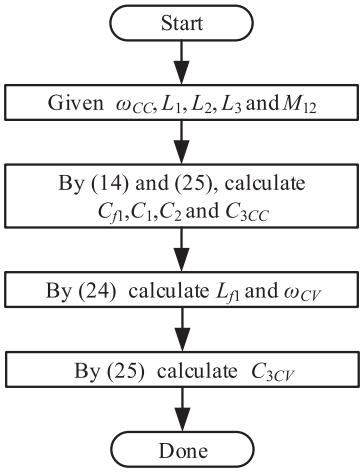

Fig. 5. Parameter design process of proposed WPT system.

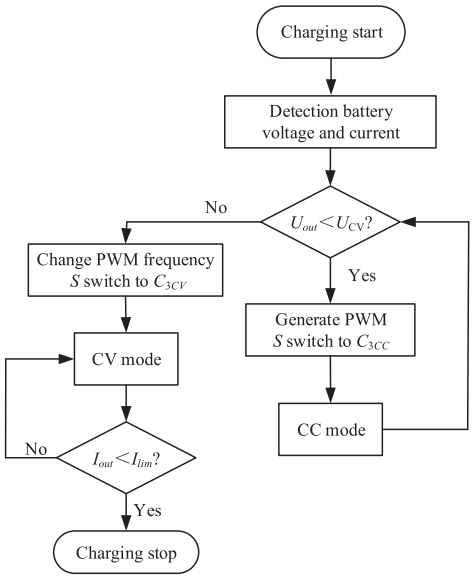

Fig. 6. Switching control flowchart of CC/CV charging stages.

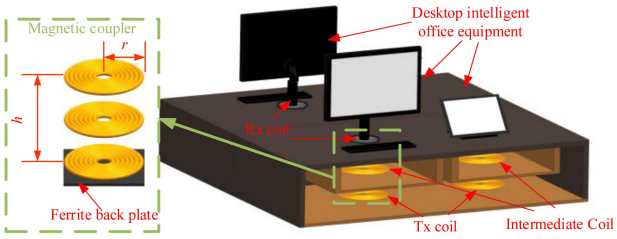

Fig. 7. Proposed WPT system in mobile desktop charging.

Fig. 6 exhibits the control flowchart of CC/CV two-stage charging procedure for the proposed WPT system. In the initial charging procedure, pulsewidth modulation (PWM) signal with frequency of ω_{CC} is generated to control switch S_1-S_4, and switch S to C_{3CC}, the CC charging mode starts. The CV charging stage

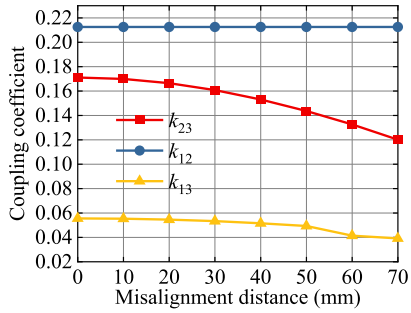

Fig. 8. Variations of k_{12}, k_{23}, and k_{13} with *Rx* coil misalignment.

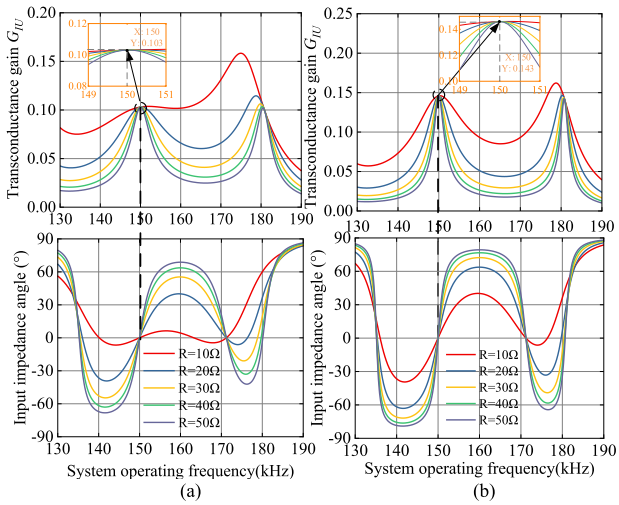

Fig. 9. CC charging mode. (a) Transconductance gain and input impedance angle at $k_{23} = 0.17$. (b) Transconductance gain and input impedance angle at $k_{23} = 0.12$.

begins as the load voltage U_{out} reaches the upper voltage limit U_{CV}, change the PWM signal frequency to ω_{CV} and switch S to C_{3CV}, simultaneously. Finally, the whole charging process ends at the moment that the load current I_{out} drops to the lower limit current I_{lim}.

III. Magnetic Coupling Structure and Verification

A. Magnetic Coupling Structure

The research in this article aims at the WPT system with intermediate coil over long power transmission distance in mobile desktop charging application and the receiver is designed as a wireless monitor, as shown in Fig. 7. To simply verify the feasibility of the proposed WPT system, the dense winding of circular structure is adopted for three coils, and all are of same size. Among them, *Rx* coil is integrated in the circular base of the wireless monitor (radius $r = 110$ mm). *Tx* coil with ferrite back plate is installed near the bottom of table, and the distance h between *Rx* coil and *Tx* coil is 200 mm. In addition, in order to balance aesthetics and practicality, the intermediate coil is set in the drawer mezzanine.

TABLE I
MAGNETIC COUPLER PARAMETERS

Parameters	Specification	Value
L_1	Self-inductance of *Tx* coil	265.68 μH
L_2	Self-inductance of intermediate coil	86.842 μH
L_3	Self-inductance of *Rx* coil	88.609 μH
R_1	Internal resistance of *Tx* coil	210 mΩ
R_2	Internal resistance of intermediate coil	130 mΩ
R_3	Internal resistance of *Rx* coil	90 mΩ

Fig. 8 shows the coupling coefficients between coils vary with horizontal misalignment of *Rx* coil. The self-inductance and internal resistance of three coils are given in Table I. In addition, magnetic coupler with circular structure has the same mutual inductance variation trend in all directions [24]. As displayed in Fig. 8, the misalignment of *Rx* coil would result in the variation of k_{23} between 0.12∼0.17. In contrast, k_{12} remains stable when the Rx coil is misaligned. Besides, k_{13} always maintain at a low value, coupling between *Tx* and *Rx* coil can be ignored at this distance [22].

B. Verification of CC and CV Charging Mode With ZPA Characteristic

Considering the electromagnetic leakage problem and the power loss from skin effect caused by excessive system resonant frequency, f_{CC} is set to 150 kHz in the CC charging mode. Besides, under this frequency, the output characteristics of the system is slightly impacted by the internal resistance of the passive components. By the parameter design process in Fig. 5, the system specification and parameters can be determined. When the system operates under CC mode, the transconductance gain G_{IU} and input impedance angle vary with operating frequency under different load resistance are acquired. The results, as Fig. 9 displays, are used to verify the CC output characteristic under ZPA operation.

It can be inferred from Fig. 9, when the load resistance is different, the change trend of transconductance gain and input impedance angle with frequency are distinct. However, the values of transconductance gain and input impedance angle keep constant, when the system operating frequency is 150 kHz. At this frequency under CC charging pattern, the ZPA operation is achieved. Meanwhile, it is indicated that the change of k_{23} does not affect input impedance angle, by comparing Fig. 9(a) and (b).

Similarly, for verifying CV output characteristic with ZPA operation, Fig. 10 demonstrates the tendency of voltage gain G_{UU} and input impedance angle vary with load resistance and frequency. The results show that when the system operating frequency is 171.1 kHz, the voltage gain and input impedance angle are fixed. Thus, CV output characteristic is achieved under this frequency. In addition, the ZPA characteristic has nothing with coupling coefficient k_{23} by observing Fig. 10(a) and (b).

C. Stiffness Analysis of Proposed WPT System

The WPT system's output characteristics are remarkably impacted by the parameter values of compensation components.

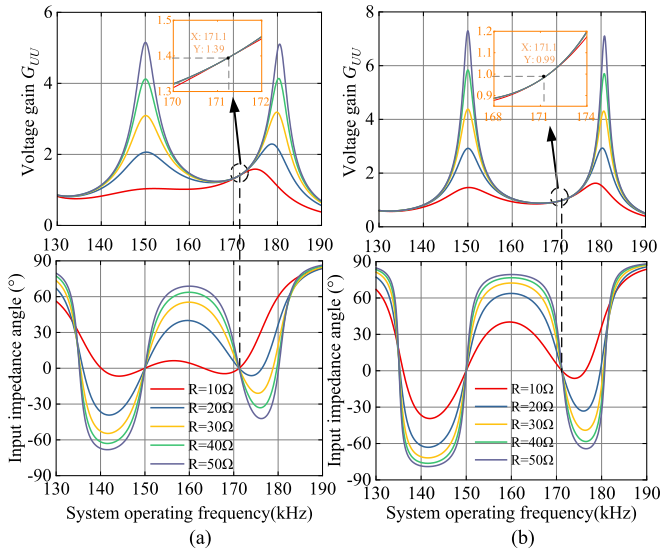

Fig. 10. CV charging mode. (a) Voltage gain and input impedance angle at $k_{23} = 0.17$. (b) Voltage gain and input impedance angle at $k_{23} = 0.12$.

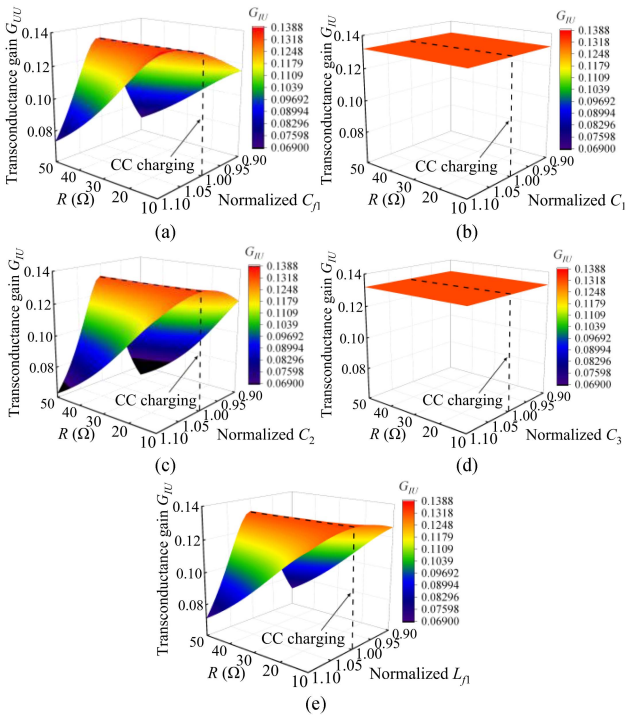

Fig. 11. Stiffness analysis in CC charging mode. (a) Deviation of C_{f1}. (b) Deviation of C_1. (c) Deviation of C_2. (d) Deviation of C_3. (e) Deviation of L_{f1}.

In order to investigate the effects of different compensation components on system's output characteristics, the parameters of C_{f1}, C_1, C_2, C_3, L_{f1} are all normalized. In this article, the load resistance *R* varies from 10 to 50 Ω, and normalized values of compensation components range from 0.9 to 1.1.

When each compensation element deviates from the preset value, the relationship between transconductance gain and load resistance is shown in Fig. 11. By observing Fig. 11(a)

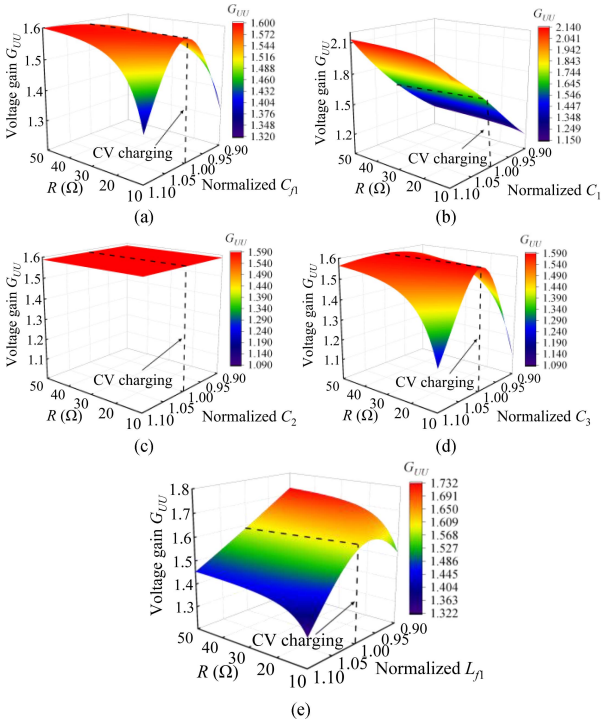

Fig. 12. Stiffness analysis in CV charging mode. (a) Deviation of C_{f1}. (b) Deviation of C_1. (c) Deviation of C_2. (d) Deviation of C_3. (e) Deviation of L_{f1}.

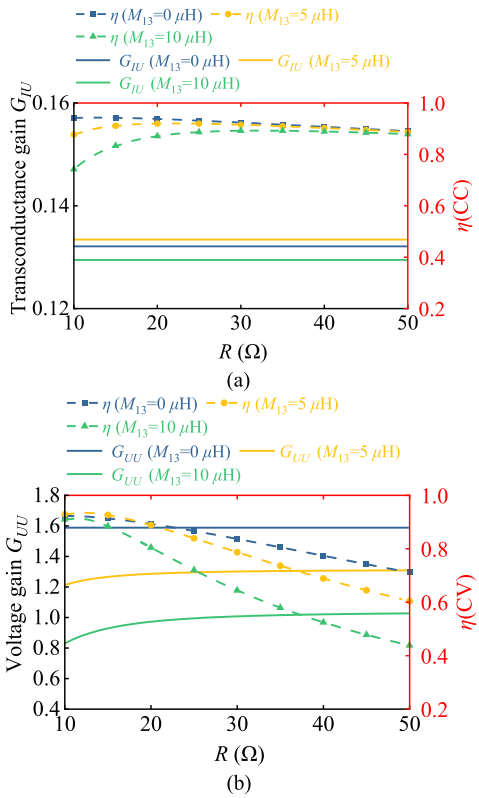

Fig. 13. Influence of cross coupling on system's output characteristics. (a) CC mode. (b) CV mode.

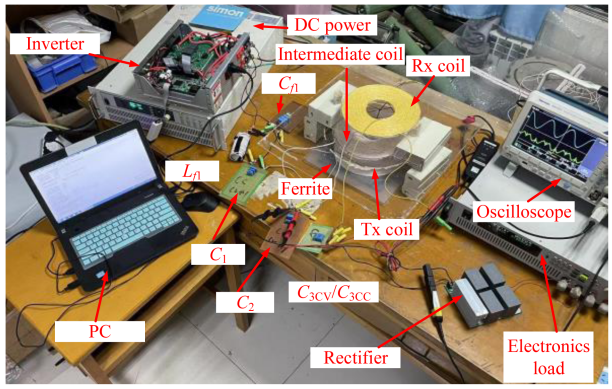

Fig. 14. Experimental prototype of the proposed WPT system.

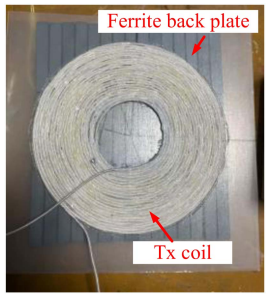

Fig. 15. Proposed *Tx* coil with ferrite.

and (c), it can be inferred that in CC charging mode, the configuration accuracy of C_{f1} and C_2 has a significant influence on the transconductance gain G_{IU}, in other words, during compensation parameter configuration, should pay special attention to the values of C_{f1} and C_2. In contrast, the compensation parameters C_1 and C_3 have less effect on the transconductance gain G_{IU}. Meanwhile, the influence of the configuration error of compensation inductance L_{f1} on the WPT system's CC output characteristics is shown in Fig. 11(e), its influence law is similar to C_{f1} and C_2.

Similarly, the stiffness analysis in CV charging mode is shown in Fig. 12. By surveying Fig. 12(a), (b), and (d), it can be indicated that the system's CV output characteristics are remarkably influenced by the variations in compensation components C_{f1}, C_1, C_3. On the contrary, the change of compensation capacitance C_2 rarely affects the voltage gain. Besides, by Fig. 12(e), in the process of configuring compensation inductor L_{f1}, improper deviation will affect the CV characteristic.

In summary, improper operation in parameter configuration process of compensation components will cause the output to deviate from the preset value, and the accuracy of each compensation component should be guaranteed.

D. Validity Analysis of Ignoring Cross Coupling M_{13}

In the above analysis, the cross coupling M_{13} is ignored. The influence of cross coupling M_{13} on output characteristics of

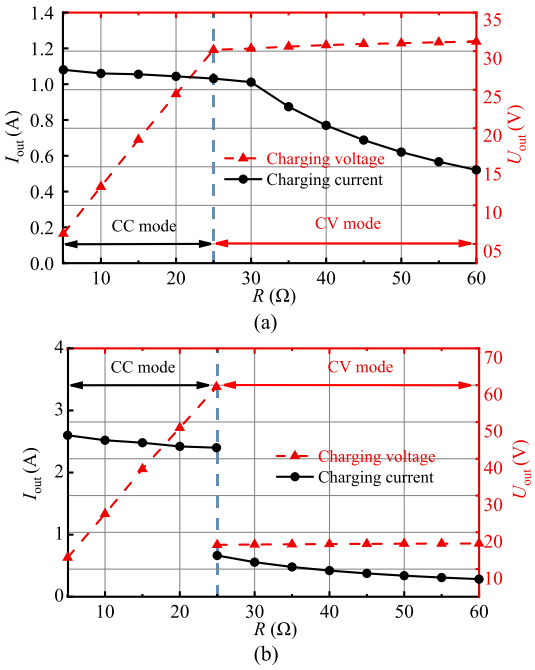

Fig. 16. Whole charging process. (a) $k_{23} = 0.17$. (b) $k_{23} = 0.12$.

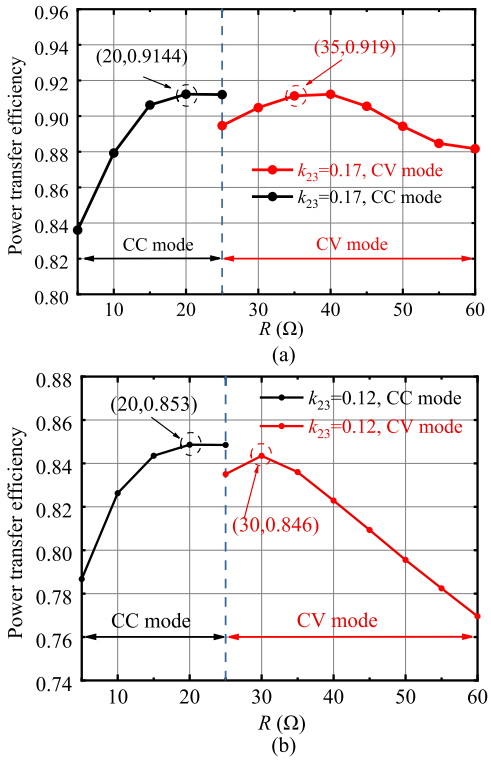

Fig. 17. Power transfer efficiency of the proposed WPT system during the whole charging process under different coupling coefficients. (a) $k_{23} = 0.17$. (b) $k_{23} = 0.12$.

proposed WPT system is studied to analyze the validity. The influence law is exhibited in Fig. 13.

As exhibited in Fig. 13(a), although M_{13} will not affect the CC output characteristics, the power transfer efficiency η(CC) will decrease with the increase of cross coupling M_{13}, especially when load resistance is small. For system operating in CV charging mode, excessive cross-coupling M_{13} will change the CV output characteristics, significantly. In contrary with CC mode, M_{13} will cause power transfer efficiency η(CV) to decrease rapidly when load resistance is at large value as shown in Fig. 13(b). However, the proposed system has certain stiffness when cross coupling exists, system can still maintain efficient and stable output in the case of proper value of M_{13}. The analysis proved that the ignoring of cross coupling M_{13} is reasonable when cross coupling keeps at small value. In the proposed system with magnetic coupler parameters of Table I, the cross coupling M_{13} is 6.1 μH, it can be ignored.

IV. Experimental Verification

To proving the feasibility of above theoretical analysis and validating the superiority of *LCC-S-S* compensated three-coil WPT system, an experimental prototype is implemented and tested. It is displayed in Fig. 14. The inverter is composed of four MOSFETs (GS66508B), the rectifier is made up of four diodes (IV1D12030U3). The variation of load resistance is simulated by electronics load. Besides, during the winding process of magnetic coupler, the Litz wires with a diameter of approximately 4 mm are adopted, thus the skin effect can be relieved. The size of PC40 ferrite core is introduced to enhance the magnetic coupling. Fig. 15 shows the *Tx* coil with ferrite. In addition, Table II gives the proposed system's specification and designed parameters, including the compensation parameters and operating frequencies.

TABLE II
System Specification and Designed Parameters

Parameters	Specification	Value
L_{f1}	Compensation inductance	24.39 μH
C_{f1}	Compensation capacitance	46.15 nF
C_1	Capacitor of *Tx* side	4.66 nF
C_2	Capacitor of intermediate side	12.29 nF
C_{3CC}	Capacitor of Rx side in CC mode	12.70 nF
C_{3CV}	Capacitor of Rx side in CV mode	9.77 nF
f_{cc}	Operating frequency in CC mode	149.5 kHz
f_{cv}	Operating frequency in CV mode	178.7 kHz

In the setting of this experiment, when the WPT system operates under CC charging pattern, the range of load resistance R is between 5 to 25 Ω. Subsequently, the charging procedure changes to CV mode, while load resistance varies from 25 to 60 Ω. During the whole charging process, the measured charging current and voltage are demonstrated in Fig. 16.

According to Fig. 16(a), when *Rx* coil is aligned, i.e., $k_{23} = 0.17$, the fluctuation of charging current I_{out} under CC pattern is no more than 5.7% and the variation of charging voltage U_{out} is below 2.9% under CV charging stage. It has indicated that the proposed *LCC-S-S* compensated three-coil WPT system has an agreeable CC/CV output characteristic under different load resistance, which could meet the demand of CC/CV two-stage

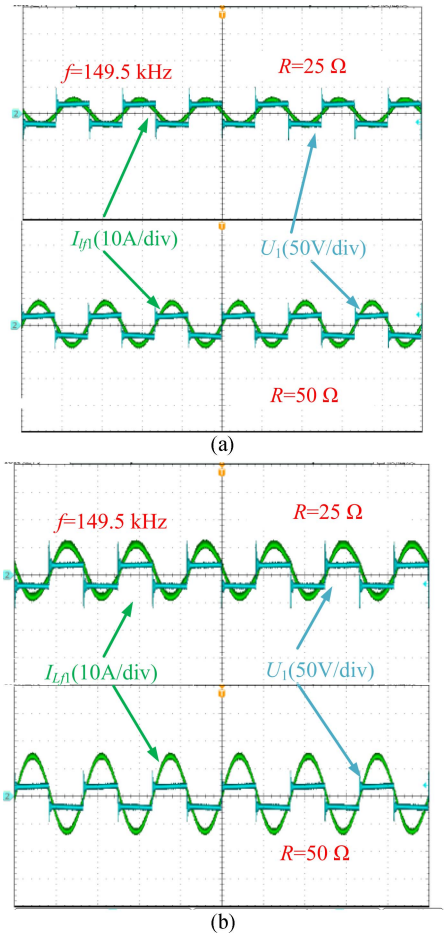

Fig. 18. Waveforms of input current I_{Lf1} and input voltage U_1 in the CC charging mode. (a) $k_{23} = 0.17$. (b) $k_{23} = 0.12$.

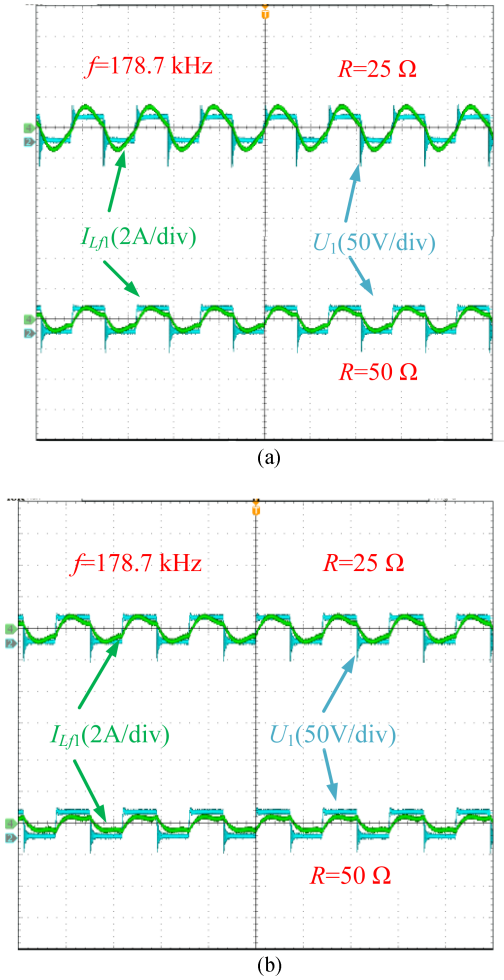

Fig. 19. Waveforms of input current I_{Lf1} and input voltage U_1 in the CV charging mode. (a) $k_{23} = 0.17$. (b) $k_{23} = 0.12$.

charging for batteries. By comparing Fig. 16(a) and (b), and combing (15) and (26), it can be demonstrated k_{23} will affect the transconductance gain G_{IU} under CC pattern and voltage gain G_{UU} under CV stage. However, when the Rx coil is misaligned, i.e., $k_{23} = 0.12$, the fluctuation of charging current I_{out} is under 8%, at the same time, the maximum variation of charging voltage U_{out} is 2.1%. It should be noted that under the misaligned situation, the charging current and voltage are different from the values when *Rx* coil is aligned. It could be indicated from Fig. 16(b) that a sudden change in charging current and voltage also cause troubles to the battery charging. In order to solve this problem, in further study, a simple phase-shift control method is going to be added in the *Tx* side to adjust U_1 under misalignment situation. Thus, the desired charging current and voltage could be met according to (17) and (28).

During the whole charging process, the proposed WPT system's power transfer efficiency under different coupling coefficients is demonstrated in Fig. 17. When *Rx* coil is aligned, the power transfer efficiency increases from 83.8% to 91.4% in the CC charging mode and then gradually arises, the maximum power transfer efficiency of the proposed system reaches 91.9%, it slowly drops at the end of CV charging mode, as shown in Fig. 17(a). When misalignment occurs, the power transfer

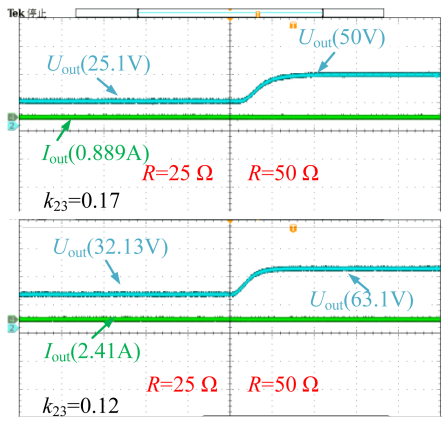

Fig. 20. Waveforms of output voltage and current at the moment of load resistance switching in CC mode.

efficiency climbs up from 78.8% to 85.3% in CC charging pattern and at the beginning of CV charging stage, the efficiency of system increases from to 83.5% to 84.6%, after that the power transfer efficiency decreases gradually during the remaining charging process. It is manifest that the misalignment of *Rx*

TABLE III
COMPARISON STUDY WITH THE RELEVANT WORKS

References	Li et al. [7]	Liu et al. [16]	Yang et al. [20]	Li et al. [25]	This article
Topology	*S-S-S*	S-hybrid C-dual S	*S-S-P*	S-hybrid C- S	*LCC-S-S*
Magnetic coupler layout	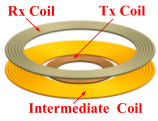	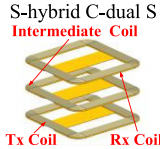	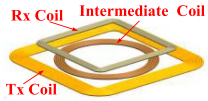	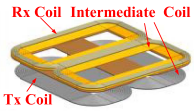	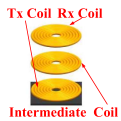
Tx coil size	diameter=200 mm (circular)	300×300 mm(Q) 215×60 mm (DD)	300×300 mm(Q)	150×150 mm(DD)	diameter=220 mm (circular)
Intermediate coil size	diameter=400 mm (circular)	300×300 mm(Q) 215×60 mm (DD)	diameter=150 mm (circular)	150×150 mm(DD1) 150×150 mm(DD2)	diameter=220 mm (circular)
Rx coil size	diameter=400 mm (circular)	300×300 mm(Q) 215×60 mm (DD)	160×160 mm (Q)	150×150 mm (DD)	diameter=220 mm (circular)
Power transfer distance	200 mm	200 mm	65 mm	20 mm	200mm
Total number of compensation component	6	8	3	4	5
Number of AC switches	2	2	/	2	1
Frequency in CC mode	200 kHz	85 kHz	76.25 kHz	500kHz	149.5 kHz
Frequency in CV mode	200 kHz	85 kHz	66.25 kHz	500kHz	178.7 kHz
ZPA in CC mode with misalignment	YES	YES	YES	YES	YES
ZPA in CV mode with misalignment	YES	YES	NO	YES	YES
Power transmission efficiency	81.1%~90.8%@CC 90.8%~53.1%@CV	94.1%~89.2%@CC 89.2%~80.2%@CV	91.8%~94.2%@CC 96.0%~91.9%@CV	90%~92.25%@CC 92.25%~77%@CV	83.8%~91.4%@CC 91.9%~88%@CV
Compact/ lightweight on *Rx*	NO	NO	YES	YES	YES
Suitable for long-distance WPT system	NO	NO	NO	NO	YES

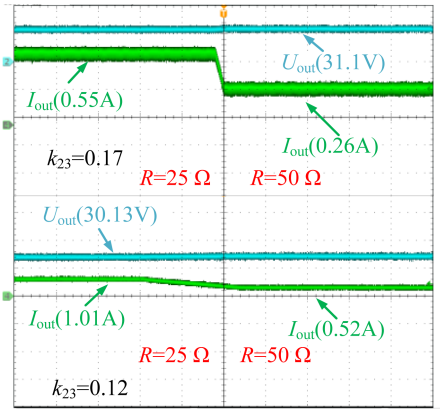

Fig. 21. Waveforms of output voltage and current at the moment of load resistance switching in CV mode.

coil will cause the decrease of power transfer efficiency, by comparing Fig. 17(a) with (b).

The waveforms of input current and input voltage in CC charging mode with different load resistance under coupling coefficient $k_{23} = 0.17, 0.12$ are show in Fig. 18(a) and (b), respectively. It can be concluded that the change of load resistance R and coupling coefficient k_{23} will not affect the phase angle between input current and input voltage.

Similar analysis can also be obtained in the CV charging mode from Fig. 19(a) and (b), the ZPA characteristics of the system have been verified.

In addition, the output voltage U_{out} and output current I_{out} waveforms in CC charging pattern at the moment when the load resistance is switched from 25 to 50 Ω are demonstrated in Fig. 20. At the moment of switching, the output current is almost unchanged, while the output voltage becomes twice as much as before switching. The above characteristics can be achieved at $k_{23} = 0.17$ and 0.12. Thus, the CC charging mode has been verified.

Similarly, the output voltage U_{out} and output current I_{out} waveforms in CV charging pattern at the moment when the load resistance is switched from 25 to 50 Ω are exhibited in Fig. 21. The instantaneous output voltage remains almost constant at the moment of switching, while the load current drops by half, when $k_{23} = 0.17$ and 0.12. Table III gives the comparison results with the relevant works from eight aspects. It can be concluded from Table III that the proposed WPT system with *LCC-S-S* compensation in this article has the following advantages. First, the compensation components and ac switches integrated in proposed WPT system are relatively few, especially at *Rx* side. Secondly, the proposed *LCC-S-S* compensated three-coil WPT system with CC/CV output characteristics is suitable for long-distance power transmission. Last but not least, with the proposed method, ZPA operation could be obtained in CC and CV charging stages in the event of misalignment between the magnetic coupler.

V. CONCLUSION

This article proposes a switchable dual-frequency *LCC-S-S* topology with CC/CV output characteristic and ZPA conditions for the application of three-coil WPT system in mobile desktop charging with long distance. CC and CV output characteristics are acquired under two constant operation frequencies, and the charging modes are converted by switching compensation capacitor connected in series with the *Rx* coil. The stiffness analysis of compensation components on the output characteristic is

presented in this article. Experimental results demonstrate that the fluctuation of charging current with load resistance change under CC pattern is no more than 5.7% and the variation of charging voltage is below 2.9% under CV charging stage, when the *Rx* coil is aligned. The maximum and minimum power transfer efficiencies are 91.9% and 83.8%. Furthermore, the ZPA conditions can be maintained under different coupling coefficients.

REFERENCES

[1] A. U. Ibrahim, W. Zhong, and M. D. Xu, "A 50-kW three-channel wireless power transfer system with low stray magnetic field," *IEEE Trans. Power Electron.*, vol. 36, no. 9, pp. 9941–9954, Sep. 2021.

[2] M. Budhia, J. T. Boys, G. A. Covic, and C.-Y. Huang, "Development of a single-sided flux magnetic coupler for electric vehicle IPT charging systems," *IEEE Trans. Ind. Electron.*, vol. 60, no. 1, pp. 318–328, Jan. 2013.

[3] C. Xiao, K. Wei, D. Cheng, and Y. Liu, "Wireless charging system considering eddy current in cardiac pacemaker shell: Theoretical modeling, experiments, and safety simulations," *IEEE Trans. Ind. Electron.*, vol. 64, no. 5, pp. 3978–3988, May 2017.

[4] J. Wang et al., "Misalignment-tolerant integrated IPT systems for tram logistics robots featuring dual-purpose coupler," *IET Electric Power Appl.*, vol. 14, pp. 1984–1995, 2020.

[5] Q. Zhu, M. Su, Y. Sun, W. Tang, and A. P. Hu, "Field orientation based on current amplitude and phase angle control for wireless power transfer," *IEEE Trans. Ind. Electron.*, vol. 65, no. 6, pp. 4758–4770, Jun. 2018.

[6] L. Xun, "Qi Standard wireless power transfer technology development toward spatial freedom," *IEEE Circuits Syst. Mag.*, vol. 15, no. 2, pp. 32–39, 2015.

[7] Y. Li, Q. Xu, T. Lin, J. Hu, Z. He, and R. Mai, "Analysis and design of load-independent output current or output voltage of a three-coil wireless power transfer system," *IEEE Trans. Transp. Electrific.*, vol. 4, no. 2, pp. 364–375, Jun. 2018.

[8] J. Zhang, X. Yuan, C. Wang, and Y. He, "Comparative analysis of two-coil and three-coil structures for wireless power transfer," *IEEE Trans. Power Electron.*, vol. 32, pp. 341–352, Jan. 2017.

[9] X. Qu, H. Han, S.-C. Wong, K. T. Chi, and W. Chen, "Hybrid IPT topologies with constant current or constant voltage output for battery charging applications," *IEEE Trans. Power Electron.*, vol. 30, no. 11, pp. 6329–6337, Nov. 2015.

[10] C. S. Wang, O. H. Stielau, and G. A. Covic, "Design considerations for a contactless electric vehicle battery charger," *IEEE Trans. Ind. Electron.*, vol. 52, no. 5, pp. 1308–1314, Oct. 2005.

[11] H. H. Wu, A. Gilchrist, K. D. Sealy, and D. Bronson, "A high efficiency 5 kW inductive charger for EVs using dual side control," *IEEE Trans. Ind. Informat.*, vol. 8, no. 3, pp. 585–595, Aug. 2012.

[12] M. Fu, H. Yin, X. Zhu, and C. Ma, "Analysis and tracking of optimal load in wireless power transfer systems," *IEEE Trans. Power Electron.*, vol. 30, no. 7, pp. 3952–3963, Jul. 2015.

[13] J. Lu, W. Li, B. Li, and G. Zhu, "Variable compensation network for achieving constant current or voltage output in IPT system," in *Proc. Int. Conf. Ind. Inform.-Comput. Technol., Intell. Technol., Ind. Inf. Integr.*, 2016, pp. 14–17.

[14] Y. Chen, N. Yang, L. Liu, R. Dai, Z. He, and R. Mai, "Two/three-coil hybrid topology for WPT systems charging electric bicycles," in *Proc. IEEE Appl. Power Electron. Conf. Expo.*, 2019, pp. 3084–3087.

[15] Y. Zhang, Z. Shen, W. Pan, H. Wang, Y. Wu, and X. Mao, "Constant current and Constant voltage charging of wireless power transfer system based on three-coil structure," *IEEE Trans. Ind. Electron.*, vol. 70, no. 1, pp. 1066–1070, Jan. 2023.

[16] C. Liu, W. Pan, Z. Shen, and Y. Zhang, "A wireless charging system with dual switchable constant voltage and constant current outputs based on intermediate coils," in *Proc. IEEE Int. Power Electron. Appl. Conf. Expo.*, 2022, pp. 979–982.

[17] H. Xu, Z. Huang, Y. Yang, Z. Huang, I. W. Iam, and C. S. Lam, "Analysis and design of three-coil coupler for inductive power transfer system with automatic seamless CC-to-CV charging capability," *IEEE Access*, vol. 10, pp. 10139–10148, 2022.

[18] V.-B. Vu, D.-H. Tran, and W. Choi, "Implementation of the constant current and constant voltage charge of inductive power transfer systems with the double-sided LCC compensation topology for electric vehicle battery charge applications," *IEEE Trans. Power Electron.*, vol. 33, no. 9, pp. 7398–7410, Sep. 2018.

[19] L. Yang, X. Li, S. Liu, Z. Xu, C. Cai, and P. Guo, "Analysis and design of three-coil structure WPT system with constant output current and voltage for battery charging applications," *IEEE Access*, vol. 7, pp. 87334–87344, 2019.

[20] L. Yang, L. Ren, Y. Shi, M. Wang, and Z. Geng, "Analysis and design of a S/S/P-compensated three-coil structure WPT system with constant current and constant voltage output," *IEEE J. Emerg. Sel. Top. Power Electron.*, vol. 11, no. 3, pp. 2487–2500, Jun. 2023.

[21] Y. Zhang et al., "A hybrid compensation topology with constant current and constant voltage outputs for wireless charging system," *IEEE Trans. Transp. Electrific.*, vol. 9, no. 2, pp. 2070–2080, Jun. 2023.

[22] Y. Qu, B. Zhang, W. Gu, and X. Shu, "Wireless power transfer system with high-order compensation network based on parity-time-symmetric principle and relay coil," *IEEE Trans. Power Electron.*, vol. 38, no. 1, pp. 1314–1323, Jan. 2023.

[23] R. Beiranvand, B. Rashidian, M. R. Zolghadri, and S. M. H. Alavi, "A design procedure for optimizing the LLC resonant converter as a wide output range voltage source," *IEEE Trans. Power Electron.*, vol. 27, pp. 3749–3763, 2012.

[24] X. Zhang, C. Quan, and Z. Li, "Mutual inductance calculation of circular coils for an arbitrary position with electromagnetic shielding in wireless power transfer systems," *IEEE Trans. Transp. Electrific.*, vol. 7, no. 3, pp. 1196–1204, Sep. 2021.

[25] Y. Li et al., "Reconfigurable intermediate resonant circuit based WPT system with load-independent constant output current and voltage for charging battery," *IEEE Trans. Power Electron.*, vol. 34, no. 3, pp. 1988–1992, Mar. 2019.

Haibing Wen received the B.S., M.S., and Ph.D. degrees in naval architecture and ocean engineering from Northwestern Polytechnical University, Xi'an, China, in 2010, 2013, and 2021, respectively.

Since 2021, he has been a full-time Postdoctoral Research Fellow with the School of Electrical Engineering, Xi'an University of Technology, Xi'an, China, where he is currently a Lecturer. His research interests include wireless power transfer, including electromagnetic shielding, system optimization.

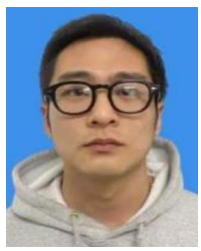

Jiayuan Li was born in Sichuan, China, in 1998. He received the B.S. degree in electrical engineering from the Hunan University of Science and Technology, Xiangtan, China, in 2020, and the M.S. degree in electrical engineering from the Xi'an University of Technology, Xi'an, China, in 2024. He is currently working toward the Ph.D. degree in electrical engineering with the Northwestern Polytechnical University, Xi'an, China.

His main research interest includes wireless power transfer.

Kehan Zhang (Member, IEEE) received the B.S. and M.S. degrees in control theory and control engineering from Northwestern Polytechnical University, Xi'an, China, in 1993 and 1996, respectively, and the Ph.D. degree in control theory and control engineering from Xi'an Jiaotong University, Xi'an, China, in 2000.

He is currently a Professor with Northwestern Polytechnical University. His research interests focus on DSP-based brushless dc motor control system and wireless power transfer.

Peng Wang received the B.S. degree in electrical engineering in 2021 from Xi'an University of Technology, Xi'an, China, where he is currently working toward the M.S. degree in electrical engineering.

His main research interest includes wireless power transfer.

Jiadong Yang received the B.S. degree in electrical engineering from Xi'an University of Posts & Telecommunications, Xi'an, China, in 2022. He is currently working toward the M.S. degree in electrical engineering with Xi'an University of Technology, Xi'an, China.

His main research interest includes wireless power transfer.

Xiaolong Zhou received the B.S. degree in electrical engineering in 2020 from Xi'an University of Technology, Xi'an, China, where he is currently working toward the M.S. degree in electrical engineering.

His main research interest includes wireless power transfer.

Lei Yang (Senior Member, IEEE) was born in Henan, China, in 1986. He received the B.S. degree in electric and information engineering from information engineering University, Zhengzhou, China, in 2011, the M.S. degree in signal and information processing, and the Ph.D. degree in electrical engineering from Northwestern Polytechnical University, Xi'an, China, in 2014 and 2017, respectively.

He is currently an Associate Professor with the Xi'an University of Technology. From 2014 to 2016, he was a Visiting Student with the University of California, Irvine, CA, USA. His research interests include nonlinear control methods, wireless power transfer systems, underwater communication, and power delivery systems, switched-capacitor converter, dc–dc converter, the power source of an electric vehicle, and renewable energy integration.

Xiangqian Tong (Member, IEEE) was born in Shaanxi Province, China, in 1961. He received the B.S. degree from the Shaanxi Institute of Technology, Hanzhong, China, in 1983, the M.S. degree in electrical engineering from Xi'an University of Technology, Xi'an, China, in 1989, and the Ph.D. degree in electrical engineering from Xi'an Jiaotong University, Xi'an, China, in 2006.

He was with the Xi'an University of Technology in 1989. Since 2002, he has been a Professor with the Xi'an University of Technology. His research interests include the application of power electronics in power system and control of power quality.

Baowei Song received the B.S. degree in mechanical engineering and the Ph.D. degree in mechatronic engineering from Northwestern Polytechnical University, Xi'an, China, in 1986 and 1999, respectively.

He is currently a Professor of Northwestern Polytechnical University. His research interests include general technical research of underwater vehicles.